Supporting Information

Distinctive phosphoinositide and Ca^{2+} binding properties of normal and cognitive performance-linked variant forms of KIBRA C2 domain

Mareike G Posner[1], Abhishek Upadhyay[1], Rieko Ishima[2], Antreas C. Kalli[3,4], Gemma Harris[5], Joachim Kremerskothen[6], Mark SP Sansom[7], Susan J Crennell[1], and Stefan Bagby[1*]

From the [1]Department of Biology and Biochemistry, University of Bath, Bath BA2 7AY; [2]Department of Structural Biology, University of Pittsburgh School of Medicine, Pittsburgh, Pennsylvania, 15260; [3]Leeds Institute of Cancer and Pathology, University of Leeds, Leeds LS9 7TF; [4]Astbury Centre for Structural Molecular Biology, University of Leeds, Leeds, LS2 9JT; [5]Research Complex at Harwell, Rutherford Appleton Laboratory, Didcot OX11 0FA; [6]Internal Medicine D, Department of Nephrology, Hypertension and Rheumatology, University Hospital Münster, Münster; [7]Department of Biochemistry, University of Oxford, Oxford OX1 3QU

Running title: *KIBRA C2: distinctive phosphoinositide and Ca^{2+} binding*

*To whom correspondence should be addressed: Stefan Bagby, Department of Biology and Biochemistry, University of Bath, Bath BA2 7AY, UK, bsssb@bath.ac.uk, Tel. 0044(0)1225 386436; Fax. 0044(0)1225 386779.

List of Supporting Information

SI Table 1. KIBRA C2 domain constructs used in this study.
SI Figure 1. Analytical ultracentrifugation sedimentation coefficient distributions of each KIBRA C2 domain construct.
SI Table 2. Species molecular weights from AUC.
SI Figure 2. ^{15}N transverse relaxation rate (R_2), ^{15}N longitudinal relaxation rate (R_1), and $\{^1H\}$-^{15}N NOE of C2(C771A).
SI Table 3. ^{15}N transverse relaxation rate (R_2), ^{15}N longitudinal relaxation rate (R_1), and $\{^1H\}$-^{15}N NOE of C2(C771A) (data used to generate SI Figure 2).
SI Figure 3. ^1H-^{15}N HSQC spectra of C771A mutant C2 and variant C771A mutant C2.
SI Figure 4. Secondary structure composition of C2(C771A) in solution and crystal.
SI Figure 5. ^1H-^{15}N chemical shift differences between C2(C771A) and varC2(C771A).
SI Figure 6. Mean density of Ca^{2+}, Asp and Glu over eight repeat simulations of C2 domain with calcium.
SI Figure 7. Chemical shift changes of seven selected residues observed in the C2(C771A)-PI(3)P titration.
SI Figure 8. Structure-based sequence alignment of C2 domains.
SI Figure 9. Sequence alignment of the C2 domain segment corresponding to the lysine-rich cluster found in some C2 domains.
SI Table 4. Data processing and refinement statistics for X-ray crystal structures.

Four human KIBRA C2 domain constructs were studied (SI Table 1): wtC2, varC2, C2(C771A) and varC2(C771A) where the variant form arises from the rs3822660G/T and rs3822659T/G minor alleles, producing two amino acid differences from wild type KIBRA C2, M734I and S735A) (1).

SI Table 1. KIBRA C2 domain constructs used in this study

Construct name and abbreviation	Plasmid and restriction sites	Residues of human KIBRA	Naturally occurring sequence variations	Mutations
Wild type C2 (wtC2)	pQE30 (BamHI/HindIII)	658-785	None	None
Variant C2 (varC2)	pQE30 (BamHI/HindIII)	658-785	M734I and S735A	None
C771A mutant C2 (C2(C771A))	pQE30 (BamHI/HindIII)	658-785	None	C771A
Variant C771A mutant C2 (varC2(C771A))	pQE30 (BamHI/HindIII)	658-785	M734I and S735A	C771A

Wild type and variant KIBRA C2 adopt a canonical C2 fold but show different self-association properties; C2(C771A) and varC2(C771A) are monomeric in solution

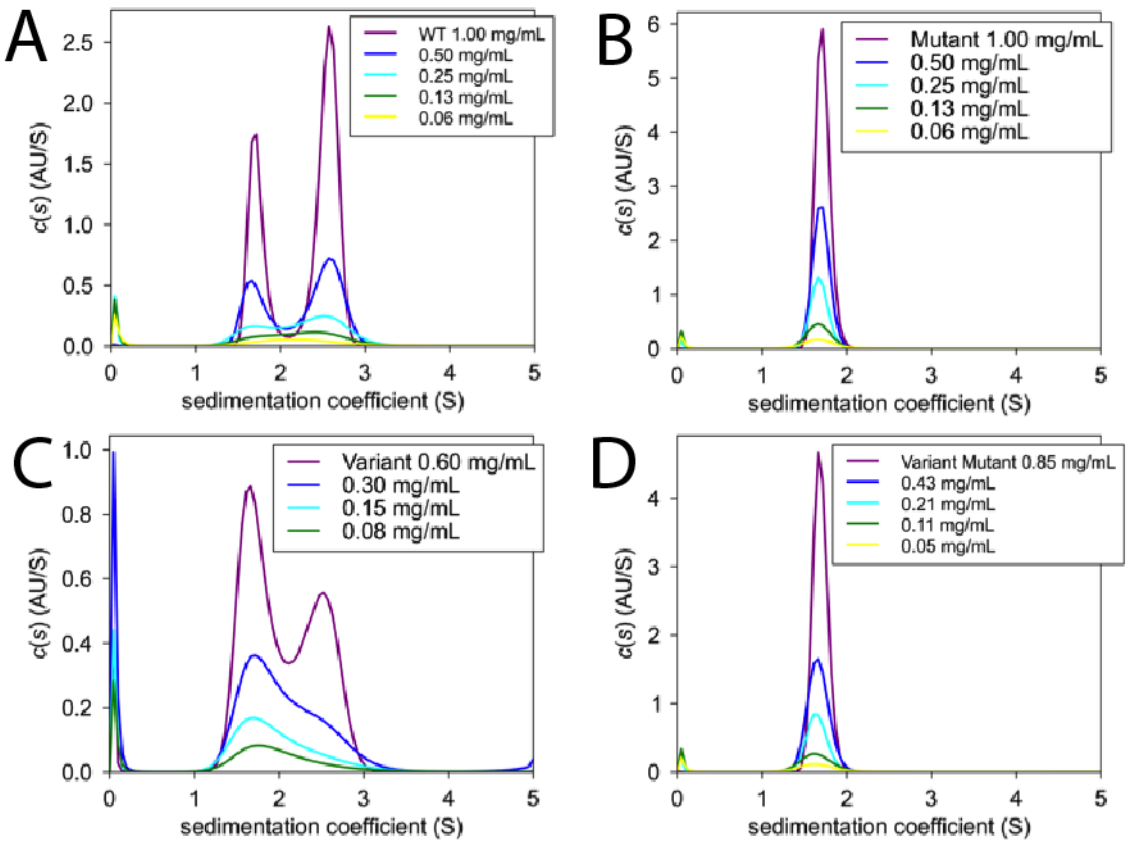

SI Figure 1. Analytical ultracentrifugation sedimentation coefficient distributions of each KIBRA C2 domain construct. (A) wtC2, (B) C2(C771A), (C) varC2, (D) varC2(C771A). The sharp peak at 0-0.2S arises from unmatched buffer salts.

SI Table 2. Species molecular weights from AUC. For each concentration, the molecular weight and sedimentation coefficient of the major species is shown, together with the best-fit frictional ratio for the distribution. *Unresolved species.

	Expected monomer MW (kDa)	Concentration (mg/mL)	Peak 1		Peak 2		f/f_0
			MW (kDa)	Sedimentation coefficient (S)	MW (kDa)	Sedimentation coefficient (S)	
wtC2	15.9	1.00	15.1	1.73	27.0	2.56	1.26
		0.50	15.3	1.73	27.3	2.54	1.27
		0.25	16.3	1.70	28.9	2.49	1.35
		0.13	23.9*	2.23*			1.33
		0.06	24.9*	2.25*			1.35
C2 (C771A)	15.8	1.00	14.6	1.72			1.24
		0.50	14.9	1.70			1.26
		0.25	15.3	1.68			1.31
		0.13	15.5	1.68			1.32
		0.06	15.8	1.68			1.34
varC2	15.8	0.60	15.7	1.74	27.0	2.49	1.28
		0.30	20.5*	2.04*			1.31
		0.15	20.5*	1.98*			1.34
		0.08	20.5*	2.03*			1.30
varC2 (C771A)	15.8	0.85	14.4	1.69			1.24
		0.43	14.7	1.68			1.27
		0.21	14.5	1.65			1.28
		0.11	15.2	1.65			1.32
		0.05	15.5	1.66			1.33

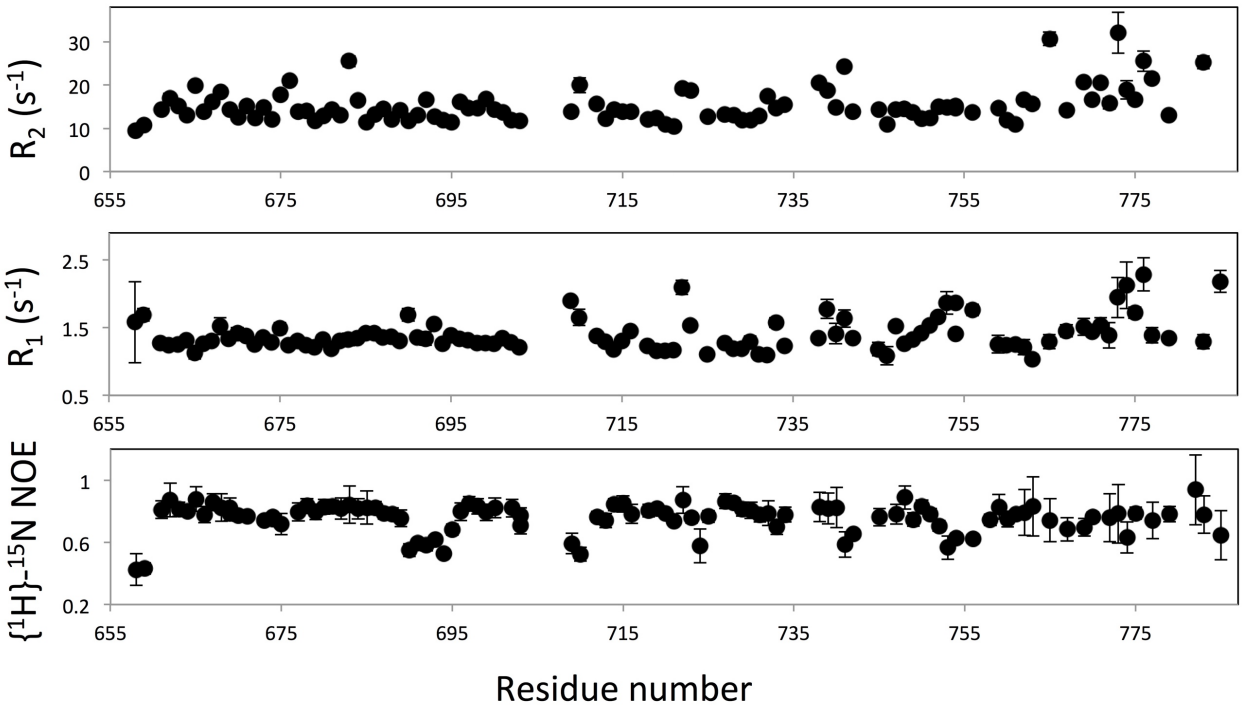

SI Figure 2. ^{15}N transverse relaxation rate (R_2), ^{15}N longitudinal relaxation rate (R_1), and {^{1}H}-^{15}N NOE of C2(C771A). Data were recorded on a cryoprobe-equipped 750 MHz spectrometer, University of Oxford, at 35°C using a uniformly ^{15}N-labelled C2(C771A) sample in 50 mM MES, 50 mM NaCl, pH 6.5. Protein concentration was 0.4 mM. R_2 and R_1 data were recorded using 10 and 14 data points with 8.9 ms to 221 ms and 0.02 s to 2.0 s relaxation periods, respectively. {^{1}H}-^{15}N NOE was recorded with 5 s pulse repetition delay. Average R_2, R_1 and NOE of a total 101 peaks were 13.8 (± 2.0) s^{-1}, 1.31 (± 0.098) s^{-1} and 0.79 (± 0.04), respectively. Among them, 42 residues that exhibit R_1 within 1.5 standard deviation against the average and NOE over 0.7 were used for estimation of the rotational correlation time. R_2, R_1 and NOE of 42 residues were fit using a simple model-free model with the local parameters, S^2 and the internal correlation time, for each residue and with a global parameter for all the residues, a rotational correlation time (2, 3). The determined rotational correlation time was 8.15 (± 0.2) ns, which reflects a 15 kDa monomer rather than the 30 kDa expected for a C2 dimer (4). This is consistent with our AUC observation (SI Fig. 1 and SI Table 2). Detailed analysis of internal dynamics was not performed due to instability of the sample (0.002 – 0.009 ppm changes during NMR experiments). Qualitatively, since both elevated R_2 and lower NOE were observed among the C-terminal 40 residues, significant dynamics occurs in the C-terminal region.

SI Table 3. ^{15}N transverse relaxation rate (R_2), ^{15}N longitudinal relaxation rate (R_1), and {^1H}-^{15}N NOE of C2(C771A) (data used to generate SI Figure 2)

AA	R_2 (s^{-1})	R_{2error} (s^{-1})	R_1 (s^{-1})	R_{1error} (s^{-1})	NOE	NOE_{error}
658	9.38	0.78	1.58	0.600	0.42	0.101
659	10.70	0.55	1.69	0.090	0.43	0.035
661	14.35	0.25	1.28	0.043	0.81	0.058
662	16.98	1.10	1.24	0.049	0.87	0.109
663	15.13	0.58	1.26	0.045	0.81	0.045
664	13.04	0.20	1.31	0.029	0.80	0.029
665	19.84	0.74	1.13	0.093	0.88	0.080
666	13.76	0.51	1.27	0.036	0.78	0.054
667	16.16	0.44	1.30	0.025	0.86	0.054
668	18.42	1.00	1.52	0.126	0.82	0.090
669	14.25	0.39	1.33	0.068	0.78	0.044
670	12.52	0.34	1.42	0.088	0.82	0.065
671	15.22	0.38	1.38	0.051	0.77	0.037
672	12.38	0.39	1.25	0.040	0.77	0.027
673	14.75	0.49	1.35	0.043	0.74	0.028
674	12.11	0.19	1.28	0.032	0.75	0.031
675	17.73	1.02	1.50	0.084	0.76	0.030
676	20.96	1.06	1.24	0.059	0.72	0.067
677	13.87	0.32	1.31	0.051	0.80	0.057
678	14.03	0.40	1.24	0.046	0.83	0.048
679	11.76	0.27	1.21	0.050	0.80	0.050
680	12.94	0.29	1.33	0.064	0.83	0.046
681	14.27	0.39	1.19	0.030	0.83	0.040
682	12.99	0.32	1.30	0.053	0.82	0.069
683	25.51	1.26	1.33	0.092	0.84	0.119
684	16.50	0.66	1.35	0.026	0.82	0.066
685	11.31	0.74	1.42	0.059	0.82	0.106
686	13.12	0.34	1.42	0.060	0.82	0.043
687	14.53	0.24	1.36	0.047	0.78	0.035
688	11.98	0.24	1.37	0.027	0.78	0.038
689	14.22	0.47	1.30	0.038	0.75	0.053
690	11.71	0.56	1.69	0.092	0.55	0.041
691	12.95	0.36	1.36	0.044	0.60	0.026
692	16.67	0.88	1.34	0.097	0.58	0.036
693	12.63	0.40	1.55	0.030	0.62	0.024
694	11.88	0.28	1.26	0.019	0.53	0.020
695	11.34	0.24	1.39	0.042	0.68	0.035
696	16.16	0.26	1.34	0.067	0.80	0.057
697	14.71	0.31	1.31	0.039	0.85	0.042
698	14.64	0.20	1.27	0.031	0.83	0.049
699	16.72	0.76	1.27	0.076	0.79	0.053
700	14.31	0.67	1.26	0.049	0.82	0.064
701	13.66	0.57	1.34	0.044	0.82	0.057
702	11.90	0.40	1.28	0.069	0.71	0.057

703	11.79	0.28	1.21	0.070	0.77	0.050
709	13.79	1.08	1.90	0.044	0.59	0.066
710	19.96	1.78	1.65	0.121	0.52	0.045
712	15.58	0.48	1.37	0.036	0.76	0.034
713	12.20	0.26	1.29	0.069	0.74	0.045
714	14.31	0.30	1.18	0.034	0.84	0.040
715	13.83	0.49	1.30	0.037	0.85	0.052
716	13.81	0.50	1.45	0.058	0.78	0.061
718	12.00	0.24	1.23	0.038	0.81	0.041
719	12.36	0.23	1.16	0.032	0.82	0.028
720	10.98	0.17	1.16	0.022	0.79	0.024
721	10.34	0.15	1.17	0.026	0.74	0.024
722	19.27	0.85	2.09	0.106	0.87	0.085
723	18.76	0.48	1.53	0.066	0.76	0.034
724	-	-	-	-	0.58	0.108
725	12.63	0.33	1.10	0.036	0.77	0.038
727	13.14	0.23	1.27	0.058	0.87	0.049
728	12.95	0.25	1.19	0.023	0.85	0.032
729	11.92	0.25	1.19	0.032	0.81	0.044
730	11.92	0.31	1.30	0.076	0.81	0.053
731	12.87	0.22	1.10	0.027	0.77	0.045
732	17.48	0.79	1.10	0.042	0.79	0.080
733	14.71	0.41	1.58	0.073	0.70	0.047
734	15.43	0.52	1.23	0.032	0.78	0.048
738	20.53	0.58	1.34	0.059	0.83	0.094
739	18.69	0.71	1.78	0.145	0.82	0.100
740	14.75	1.07	1.41	0.149	0.82	0.131
741	24.27	0.86	1.63	0.128	0.59	0.083
742	13.89	0.31	1.35	0.040	0.65	0.028
745	14.29	0.29	1.18	0.098	0.76	0.056
746	10.86	0.92	1.09	0.136	-	-
747	14.27	0.40	1.52	0.036	0.78	0.063
748	14.49	0.42	1.27	0.039	0.89	0.075
749	13.68	0.31	1.32	0.054	0.75	0.043
750	12.24	0.26	1.42	0.032	0.83	0.040
751	12.44	0.32	1.53	0.038	0.78	0.035
752	15.02	0.59	1.65	0.062	0.70	0.034
753	14.84	0.71	1.87	0.170	0.57	0.076
754	15.17	0.31	1.40	0.037	0.63	0.032
754	14.68	0.64	1.86	0.042	0.62	0.023
756	13.61	0.55	1.76	0.083	0.75	0.037
759	14.73	0.69	1.26	0.131	0.83	0.079
760	11.96	0.17	1.24	0.047	0.75	0.051
761	10.98	0.25	1.26	0.037	0.78	0.028
762	16.56	1.02	1.21	0.112	0.79	0.149
763	15.63	1.17	1.04	0.066	0.83	0.190
765	30.67	1.57	1.29	0.104	0.74	0.138
767	14.16	0.48	1.45	0.089	0.68	0.076

769	20.66	0.84	1.51	0.127	0.70	0.057
770	16.64	0.44	1.44	0.034	0.76	0.033
771	20.49	0.78	1.53	0.111		
772	15.72	1.24	1.39	0.189	0.76	0.155
773	32.05	4.73	1.95	0.298	0.78	0.190
774	18.83	2.10	2.12	0.343	0.63	0.101
775	16.64	0.45	1.72	0.082	0.79	0.039
776	25.51	2.33	2.29	0.244	0.74	0.118
777	21.55	1.12	1.39	0.116	0.78	0.049
779	12.95	0.37	1.35	0.030	0.94	0.226
783	25.25	1.51	1.29	0.109	0.78	0.121
785	-	-	2.18	0.162	0.65	0.158

C2(C771A) and varC2(C771A) samples are folded and adopt a single predominant conformation

Excellent peak dispersion and the near 1:1 ratio of the numbers of observed (124 for C2(C771A), 122 for varC2(C771A)) and expected (125, plus twelve if the N-terminal His tag is taken into account) non-side chain peaks in ^{1}H-^{15}N HSQC spectra indicate that C2(C771A) and varC2(C771A) samples are folded and adopt a single predominant conformation (SI Fig. 3). Backbone resonance assignments of C2(C771A) and varC2(C771A) were made by analysis of standard double and triple resonance NMR data sets including ^{15}N-edited TOCSY, ^{15}N-edited NOESY, HNHA, HNCACB, (CBCA)CONH, HNCO, HN(CA)CO, C(CO)NH, HC(CO)NH and HCCH TOCSY.

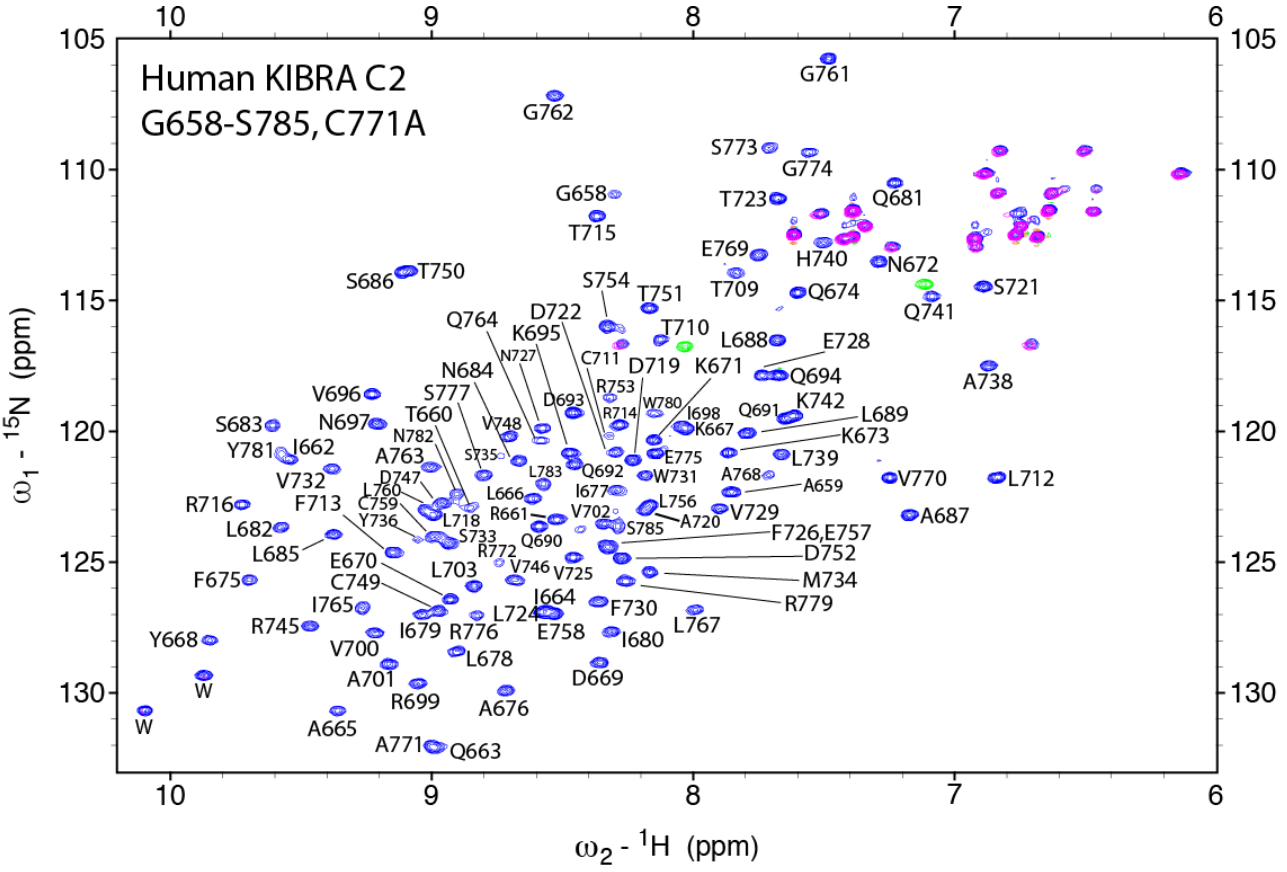

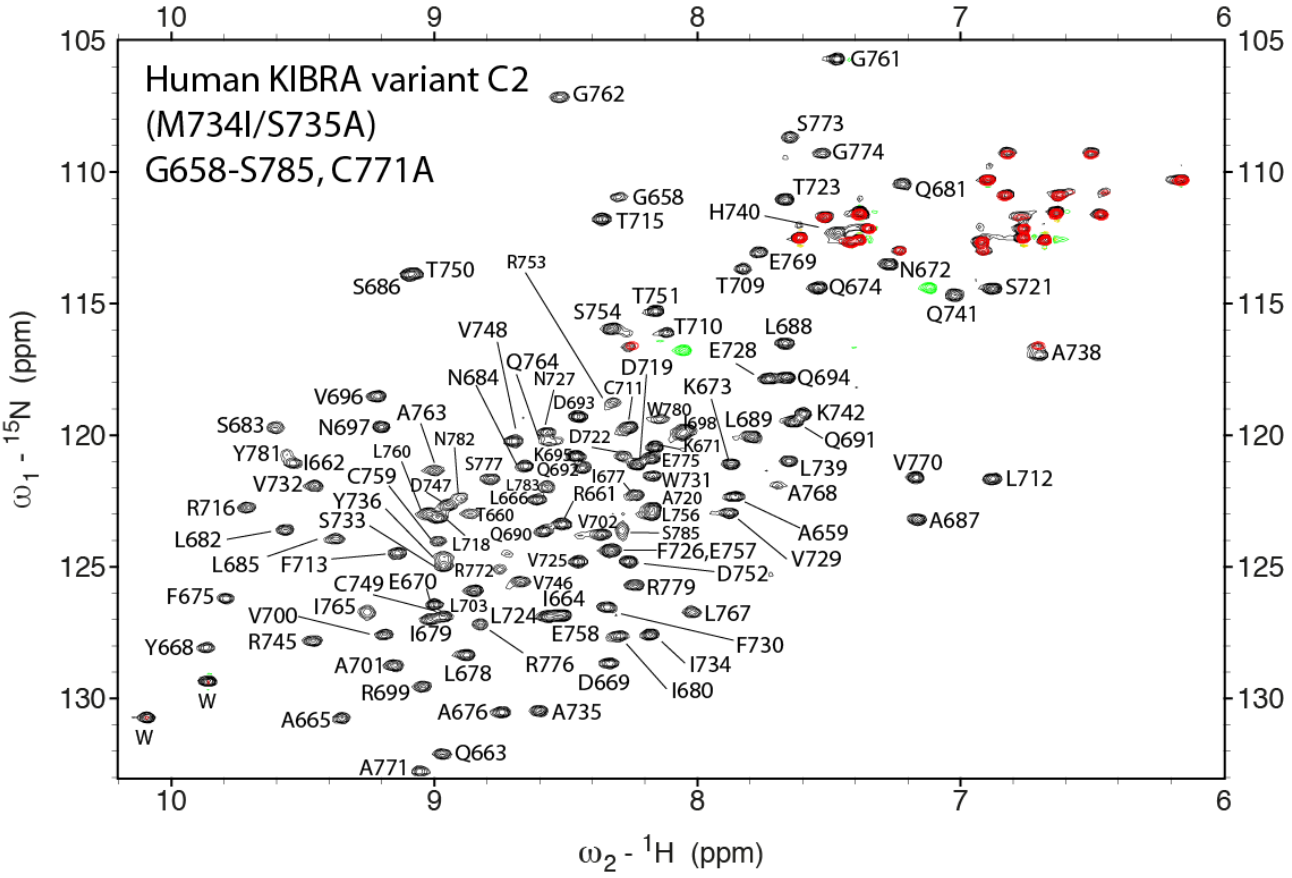

SI Figure 3. ^{1}H-^{15}N HSQC spectra of C2(C771A) and varC2(C771A). Spectra recorded with 16 scans at 35°C on a 600 MHz Varian Unity Inova spectrometer fitted with a room temperature triple resonance probe. Backbone NH peaks and side chain NH_2 peaks are shown in blue and magenta (C2(C771A)), respectively, and in black and red (varC2(C771A)), respectively. Protein concentration used for most NMR experiments was in the range 0.3 mM to 0.8 mM.

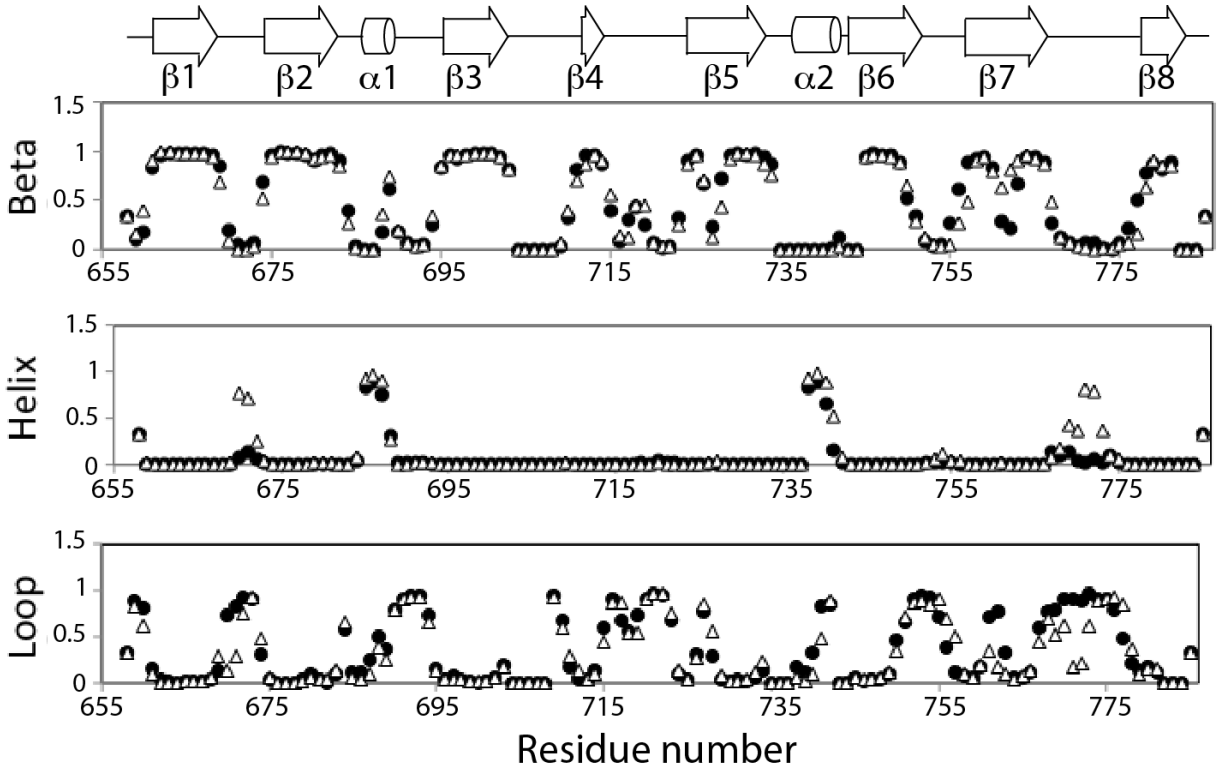

SI Figure 4. Secondary structure composition of C2(C771A) in solution and crystal. Filled circles represent the secondary structure predicted by TALOS+ (5) using C2(C771A) NMR chemical shifts from aqueous solution samples. Empty triangles represent the secondary structure predicted from our C2(C771A) crystal structure, using Sparta (6) back-calculated chemical shifts as input to TALOS+. Secondary structure element locations in the wtC2 crystal structure (PDB 2Z0U) are indicated above the histogram (arrows for β-strands, cylinders for α-helices).

NMR chemical shift differences between wild type and variant KIBRA C2 domains occur across the half of the domain distal to the CBRs

^{1}H-^{15}N chemical shift changes resulting from the two amino acid differences, M734I and S735A, between wtC2 and varC2 occur in numerous residues around the two substituted amino acids at the opposite end of the domain to the three CBRs (SI Fig. 5). The largest chemical shift differences are observed in residues V732-K742 constituting the loop and α2 between strands β5 and β6; this loop includes the two substituted residues at positions 734 and 735 which show by far the two largest chemical shift differences (SI Fig. 5B). Chemical shift differences of comparable magnitude (excluding the differences at residues 734 and 735) are also observed in and around the loop comprising residues 767-776, between strands β7 and β8 (SI Fig. 5).

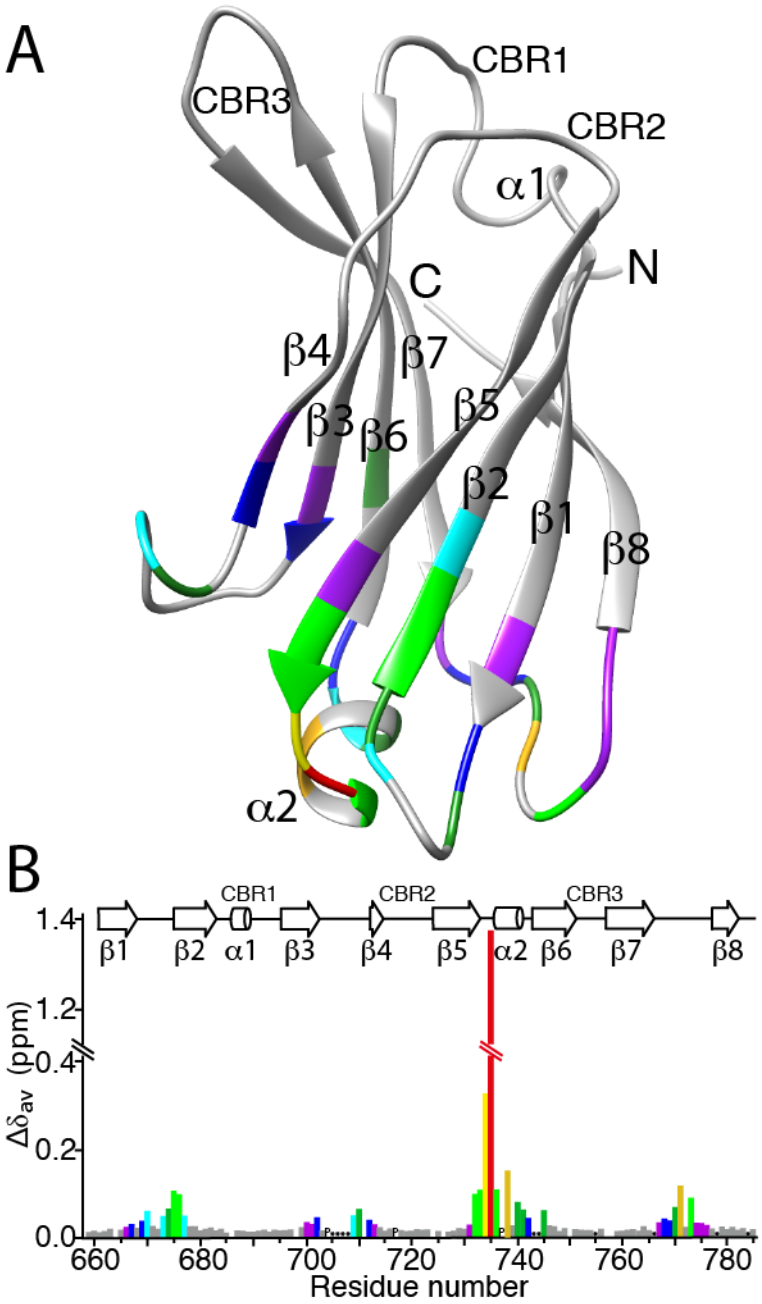

SI Figure 5. ^{1}H-^{15}N chemical shift differences between C2(C771A) and varC2(C771A). Wild type and variant C2 differ at two positions: M734 and S735 in wtC2 vs I734 and A735 in varC2. (A) Chemical shift differences mapped on to a ribbon representation of KIBRA C2 structure and (B) chemical shift differences plotted as a function of residue number. In both (A) and (B), grey represents residues with $\Delta\delta_{av}$ (ppm) ≤ 0.02, purple 0.02-0.03, blue 0.03-0.04, cyan 0.04-0.05, darker green 0.05-0.075, green 0.075-0.1, gold 0.1-0.25, yellow 0.25-0.5, orange 0.5-1.0, and red >1.0, where $\Delta\delta_{av}$ (ppm) = $[(\Delta\delta_H^2 + \Delta\delta_N^2/25)/2]^{0.5}$). In (B), P indicates proline (proline does not produce a signal in ^{1}H-^{15}N HSQC), and * indicates an unassigned residue. The secondary structure elements (β-strands, α-helices) are labelled in (A), and in (B) their locations are indicated above the histogram (arrows for β-strands, cylinders for α-helices). Also, for orientation with other C2 domains, the location of canonical calcium binding regions (CBR1, CBR2 and CBR3) is indicated.

NMR and X-ray diffraction data indicate that KIBRA C2-Ca^{2+} interaction is very low affinity and non-specific

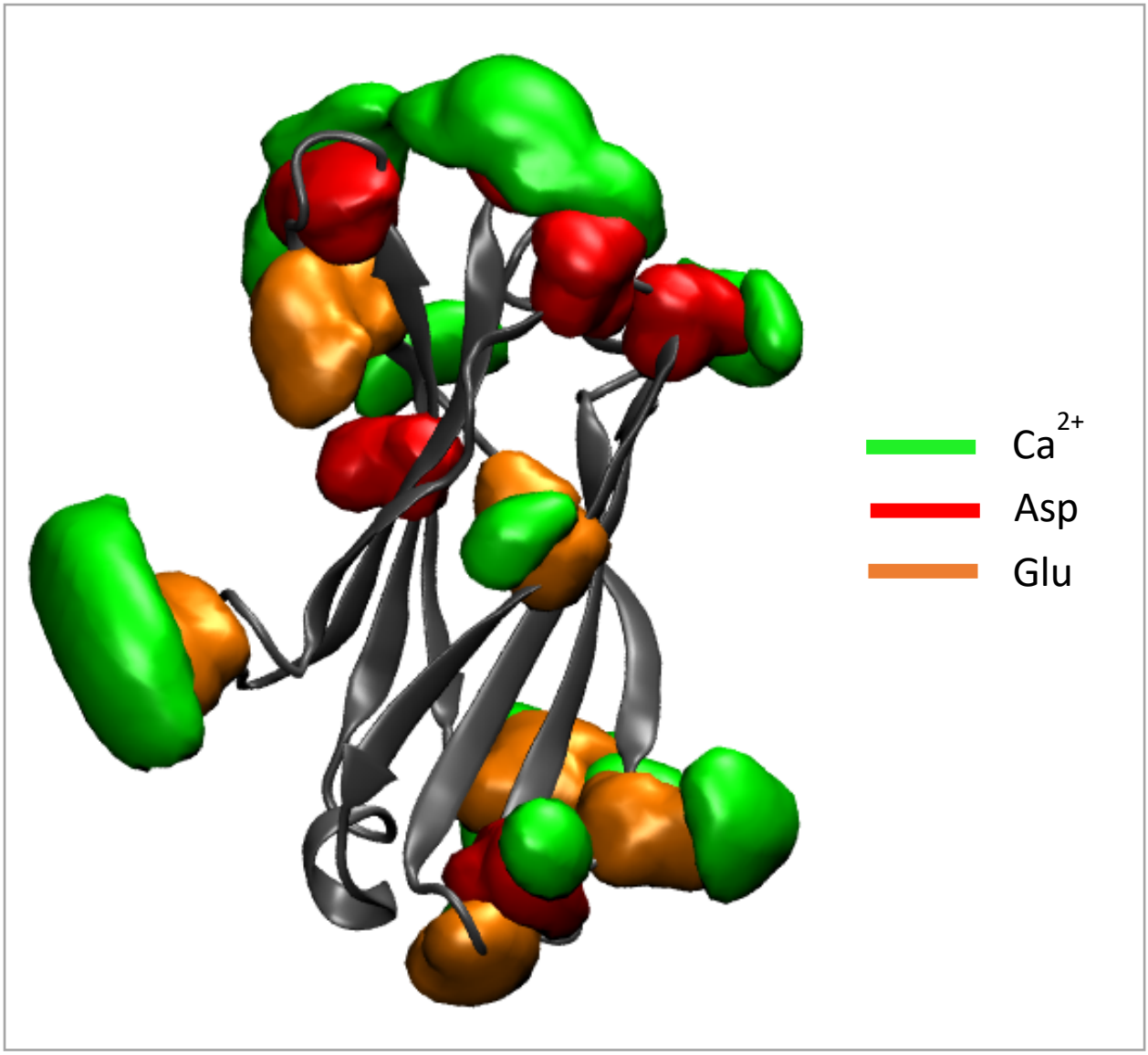

SI Figure 6. Mean density of Ca^{2+}, Asp and Glu over eight repeat simulations of C2 domain with calcium. Green denotes regions where Ca^{2+} was found frequently. Asp and Glu residue locations in red and orange, respectively.

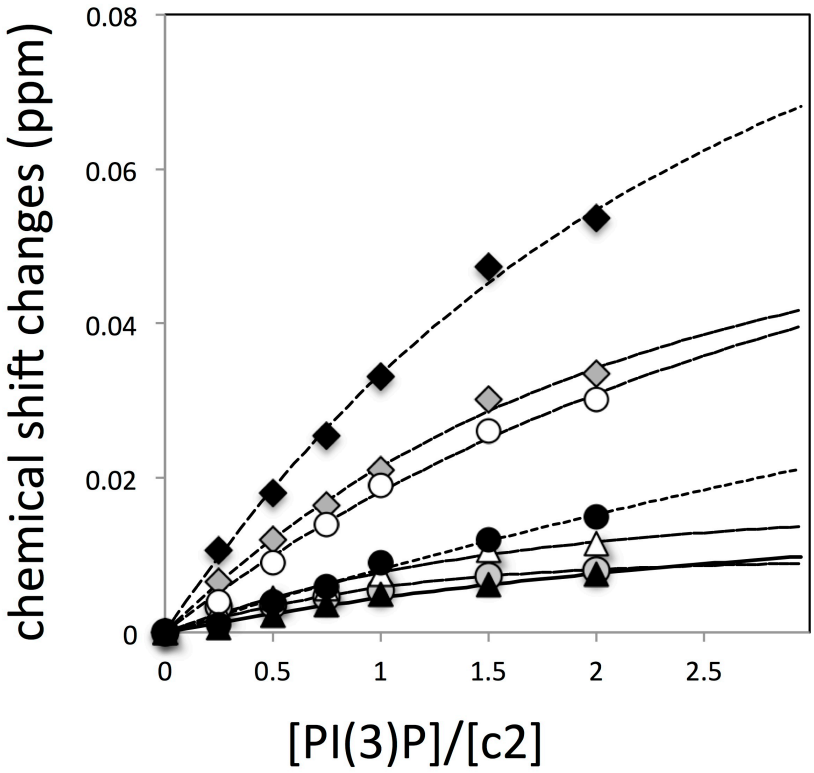

SI Figure 7. Chemical shift changes of seven selected residues observed in the C2(C771A)-PI(3)P titration shown in Figure 4. The combined chemical shifts, $[(\Delta\delta_H^2 + \Delta\delta_N^2(\gamma_N/\gamma_H))/2]^{0.5}$ (ppm), were calculated using both ^{1}H and ^{15}N shift changes, $\Delta\delta_H$ and $\Delta\delta_N$, respectively (2). Another six residues used to estimate PI(3)P dissociation constant, K_d, showed shift changes less than 0.02 ppm, and overlap with the titration points shown in the panel. Average K_d of the 13 residues was 0.97 mM (± 1.1 mM). Since the K_d is relatively high, compared for example to that of 55 μM for binding of PI(4,5)P_2 headgroup to rabphilin-3A C2A domain (7), and might depend on local environment, such as membrane composition, we did not pursue accurate K_d determination.

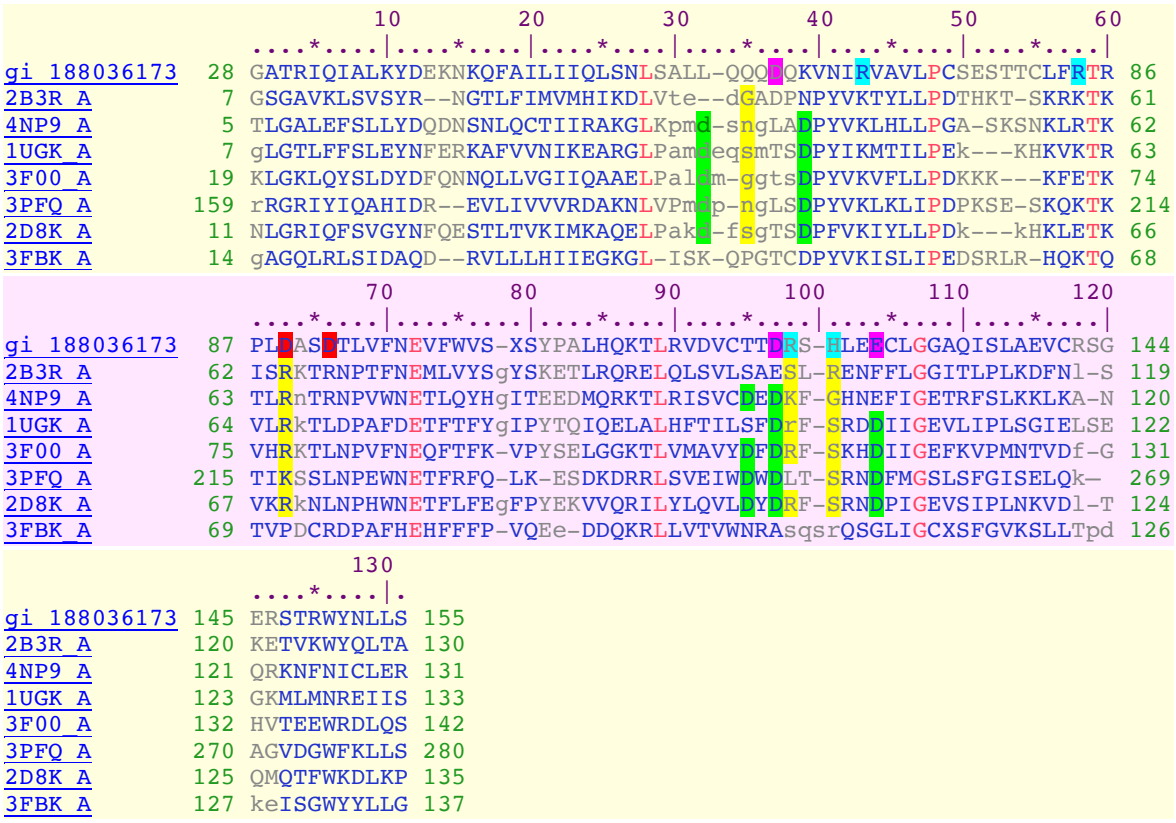

SI Figure 8. Structure-based sequence alignment of C2 domains. Based on a VAST (NCBI) search with wild type KIBRA C2 (2Z0U) as source structure (green highlight = key aspartate residues in CBR1 and CBR3 of PKCα, C2A-synaptotagmin, C2A-rabphilin, C2A-piccolo; yellow highlight = residues involved or potentially involved in lipid binding, including part of CBR2 which ends in many C2 domains with the residues NP; pink = previously proposed KIBRA C2 Ca^{2+} binding residues D693, D752, E758 (1); cyan = previously proposed KIBRA C2 phosphoinositide binding residues R699, R714, R753, H755 (1); red = KIBRA residues D719 and D722 in CBR2)

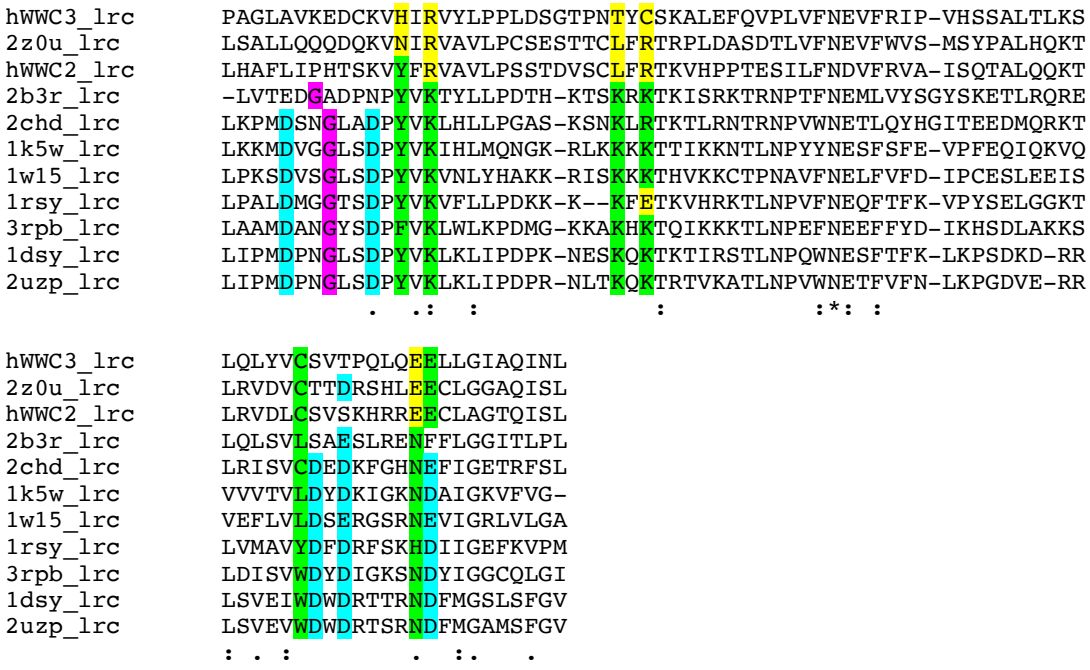

SI Figure 9. Sequence alignment of the C2 domain segment corresponding to the lysine-rich cluster found in some C2 domains. Residues of the lysine-rich cluster (abbreviated above as lrc) involved in PI(4,5)P_2 binding are highlighted in green and correspond to Y195, K197, K209, K211, W245 and N253 of PKCα. Yellow highlights where KIBRA C2 (and WWC2 and WWC3 C2) deviates from the lysine-rich cluster consensus sequence. Except for the KIBRA paralogs human WW2 and WWC3, sequences are indicated by PDB code: 2z0u = human KIBRA C2, 2b3r = phosphatidylinositide (PtdIns) 3-kinase, 2chd = rabphilin 3A C2A, 1k5w = synaptotagmin 1 C2B, 1w15 = synaptotagmin 4 C2B, 1rsy = synaptotagmin 1 C2A, 3rpb = rabphilin C2B, 1dsy = PKCα, 2uzp = PKCγ.

SI Table 4. Data processing and refinement statistics for X-ray crystal structures

	C2(C771A) (PDB 6FB4)	varC2 (PDB 6FD0)	C2(C771A) + PIP3 (PDB 6FJC)	C2(C771A) + PIP2 (PDB 6FJD)
Mutation (NB varC2 is a natural variant)	C771A	M734I/S735A	C771A	C771A
Resolution (Å)	72.6-2.42 (2.5-2.42)	50-2.62 (2.67-2.62)	72.2-2.60 (2.69-2.60)	50.0-2.9 (2.95-2.90)
Unit cell (a,b,c (Å), α,β,χ (°))	83.88, 83.88, 207.77, 90, 90, 120	34.24, 49.05, 49.5,5 62.71, 72.07, 83.71	83.37, 83.37, 208.46, 90, 90, 120	83.40, 83.40, 208.25, 90,90 120
Space group	P 6_1 2 2	P1	P 6_1 2 2	P 6_1 2 2
Rmerge	0.133 (0.625)	0.067 (0.565)	0.167 (0.621)	0.134 (0.606)
Completeness (%)	99.9 (98.6)	98.3 (86.5)	100.0 (100.0)	99.4 (98.4)
I/σ(I)	10.7 (1.7)	18.7 (1.8)	9.7 (2.3)	11.5 (2.1)
Multiplicity	10.6 (6.22)	3.6 (3.0)	12.9 (8.34)	5.8 (4.0)
Number of reflections observed	184012	161373	168296	518596
Number of unique reflections	17355	7811	13926	10159
Refinement statistics				
R_{work}	0.201	0.207	0.191	0.203
R_{free}	0.247	0.294	0.264	0.242
RMSD bond lengths (Å)	0.010	0.005	0.008	0.010
RMSD bond angles (°)	1.00	0.737	1.133	1.012
Mean isotropic B-factor (Å^2)	55.6	74.8	45.4	33.4

Molprobity protein geometry score	1.90	1.70	2.23	2.35
Molprobity clash score	3.33	5.28	5.42	4.46
PDB code	6FB4	6FD0	6FJC	6FJD

1. Duning, K., Wennmann, D. O., Bokemeyer, A., Reissner, C., Wersching, H., Thomas, C., Buschert, J., Guske, K., Franzke, V., Floel, A., Lohmann, H., Knecht, S., Brand, S.-M., Poter, M., Rescher, U., Missler, M., Seelheim, P., Boeckers, T. M., Makuch, L., Huganir, R., Weide, T., Brand, E., Pavenstädt, H., and Kremerskothen, J. (2013) Common exonic missense variants in the C2 domain of the human KIBRA protein modify lipid binding and cognitive performance. *Transl Psych*. **3**, e272
2. Cai, Y., Kurt Yilmaz, N., Myint, W., Ishima, R., and Schiffer, C. A. (2012) Differential flap dynamics in wild-type and a drug resistant variant of HIV-1 protease revealed by molecular dynamics and NMR relaxation. *J. Chem. Theory Comput.* **8**, 3452–3462
3. Webb, C., Upadhyay, A., Giuntini, F., Eggleston, I., Furutani-Seiki, M., Ishima, R., and Bagby, S. (2011) Structural Features and Ligand Binding Properties of Tandem WW Domains from YAP and TAZ, Nuclear Effectors of the Hippo Pathway. *Biochemistry* **50**, 3300–3309
4. García de la Torre, J., Huertas, M. L., and Carrasco, B. (2000) HYDRONMR: prediction of NMR relaxation of globular proteins from atomic-level structures and hydrodynamic calculations. *J. Magn. Reson.* **147**, 138–146
5. Shen, Y., Delaglio, F., Cornilescu, G., and Bax, A. (2009) TALOS+: a hybrid method for predicting protein backbone torsion angles from NMR chemical shifts. *J Biomol NMR* **44**, 213–223
6. Shen, Y., and Bax, A. (2010) SPARTA+: a modest improvement in empirical NMR chemical shift prediction by means of an artificial neural network. *J Biomol NMR* **48**, 13–22
7. Montaville, P., Coudevylle, N., Radhakrishnan, A., Leonov, A., Zweckstetter, M., and Becker, S. (2008) The PIP2 binding mode of the C2 domains of rabphilin-3A. *Protein Sci.* **17**, 1025–1034